

A COMPOSITE CYCLE ENGINE CONCEPT FOR YEAR 2050

Sascha Kaiser, Hagen Kellermann, Markus Nickl, Arne Seitz
Bauhaus Luftfahrt e.V., Taufkirchen, Germany

Keywords: Composite Cycle Engine, Propulsion Systems, Novel Cycles

Abstract

The Composite Cycle Engine concept combines the benefits of turbofan and piston engine. A highly charged piston engine operates in the high pressure part of the engine core to improve thermal engine efficiency. In this paper, the concept is applied to a year 2050 long range aircraft platform, to identify its applicability for emission reduction agendas.

Two compact and effective configurations to implement the Composite Cycle are presented, one of which features an intercooler. Methods for estimation of weight, size and emissions of such an engine are presented. A baseline concept was shown to improve fuel burn by 9.6 % over a year 2050 geared turbofan engine. The intercooled engine improves the fuel burn even more by 12.5 %. Compared to a year 2000 aircraft/engine combination, fuel burn reduces by 52 %, clearly missing the aspired 68 % improvement target. NO_x emissions in the LTO cycle are 15% higher for the baseline, but 12 % lower for the intercooled engine.

1 Introduction

Turbofan engine efficiency of projected near term engines is saturating [1]. Meanwhile, very stringent emissions reduction targets are stipulated for year 2050. The Strategic Research and Innovation Agenda [2] stipulates a 68 % mission fuel burn improvement by the aircraft/engine combination. The engine alone needs to improve by 40-48 % against year 2000 technology standard.

No concept has become the favorite for the era beyond the conventional turbofan. Therefore, the ULTIMATE project (“Ultra Low emission Technology Innovations for Mid-century Aircraft Turbine Engines”) was initiated to

screen and benchmark several candidates for improving engine efficiency [3]. Among these are intercoolers, recuperators, pulsed detonation tubes, nutating disks and low pressure technologies, such as variable pitch fans and slim line nacelles.

In this paper, the potentials of the Composite Cycle Engine (CCE) for a year 2050 technology standard engine are evaluated. The CCE concept is defined by featuring two independent sources of heat addition. The first is a piston engine operating in the high pressure core of the engine, the second a conventional combustion chamber between piston engine and turbine. The basic layout is shown in Figure 1. The High Pressure Turbine (HPT) drives the Intermediate Pressure Compressor (IPC), while the Low Pressure Turbine (LPT) drives the fan. The excess power of the Piston Engine (PE) drives a High Pressure Compressor (HPC), in this case a Piston Compressor (PC).

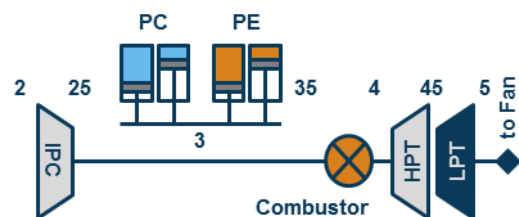


Figure 1 CCE architecture with station nomenclature [12].

The cycle diagram shown in Figure 2 illustrates the advantages of the engine: The piston cycle tops the Joule-/Brayton-cycle with much higher peak temperatures and pressures. Moreover, the combustion in the piston engine is isochoric, leading to a further pressure rise. Although the second combustor is not required when only looking for improved cycle efficiency, it helps achieving sufficient thrust under take-off

conditions and adds a degree of freedom for optimization in cruise conditions.

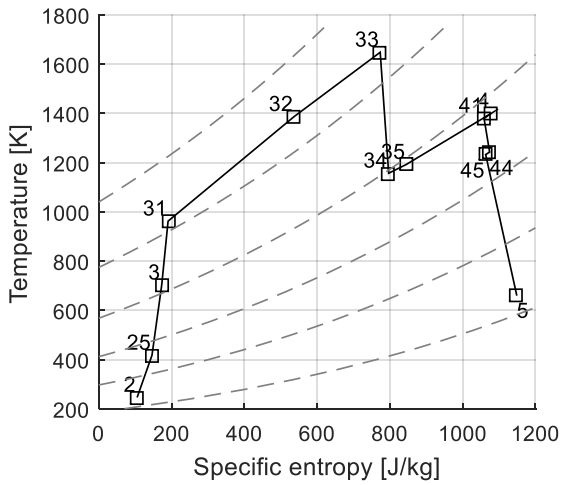


Figure 2 CCE temperature over specific entropy diagram [12].

Previous studies consistently showed double digit fuel burn improvements [4, 5, 6]. In this paper, the applicability of this concept to achieve a 15 % mission fuel burn improvement over a Geared Turbofan (GTF) with year 2050 technology standard is investigated. To this end, the CCE is conceptually designed and evaluated in the most important mission points Top of Climb (ToC), Take-off (TO) and Cruise (CR). Efficiency, weights, size and NO_x emissions are benchmarked against the reference GTF platform.

2 Studied Engine Concepts

The studied engine configuration is shown in Figure 3. The chosen HPC is an axial-radial turbo compressor. It is selected to reduce size and to guide air towards the piston engine intakes. Although a piston compressor has higher efficiency, the size was impermissibly large. The turbo shafts were consolidated into one shaft, to save weight and complexity. The added degree of freedom on the piston engine shaft is still sufficient for appropriate part-power flexibility, and to avoid problems with surge. Two V10 motors are wrapped around the engine centerline inside the core cowling. One on the bottom is implemented upside, while the top engine is hanging.

A second CCE concept investigated features an intercooler (IC) between the IPC and the HPC.

The intercooler provides several advantages to the concept. Since the piston engine is mainly thermally limited, the intercooler relaxes its design constraints. It also allows for a higher OPR, leading to a significantly smaller piston engine and lower weight.

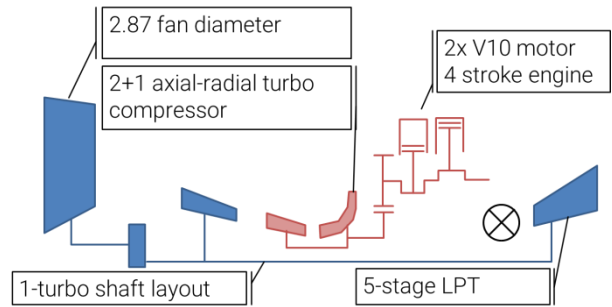


Figure 3 Baseline CCE architecture.

3 Methods

3.1 Evaluation platform

The engines presented in this paper are benchmarked on a year 2050 advanced tube and wing aircraft platform [7]. The aircraft is fully sized for a long-range mission (300 PAX, 7000 NM) for entry into service in 2050. The configuration is conventional, but advanced technologies are implemented, which improve aerodynamic efficiency and reduce operating weight empty. With an advanced geared turbofan, this configuration achieves an improvement of 45.0 % per passenger and nautical mile against year 2000 technology standard.

The geared turbofan is conceived in a similar manner in a conventional configuration, but at highly advanced technology levels. The technical specifications feature a high Overall Pressure Ratio (OPR) and Bypass Ratio (BPR). The efficiency improves by about 25 % against year 2000 technology standard. Its specifications are shown in Table 1.

The evaluation platform includes full cascading effects due to aircraft resizing, i.e. a more efficient engine leads to less fuel load with appropriately smaller wing and aircraft structure. On a long-range platform, these cascading effects are highly pronounced due to the mission length, favouring highly efficient engines.

Table 1 Main GTF operating conditions.

Parameter	ToC	TO	CR
Altitude [m]	10668	0	11278
Mach [-]	0.82	0.20	0.80
ISA dev. [K]	+10	+15	0
Thrust [kN]	50.53	185.2	32.87
T ₄ [K]	1890	1920	1540
OPR [-]	74.6	59.3	61.4
BPR [-]	16.3	16.4	17.1
TSFC [g/kN/s]	13.71	8.26	12.61

3.2 CCE Simulation

The piston engine conceptual design was conceived by using best practices from other piston engine application areas, namely high-end automotive, utility vehicle, and marine. The design choices were empirically derived and expected technological improvements until year 2050 were included [8].

The piston engine was modelled as two crankshaft connected V-type engines. One engine is located on the bottom and the other hanging on top inside the core cowling. The arrangement allows to utilize the space inside the engine efficiently, while still providing enough space for the turbo shaft inside of the perimeter of the piston engines.

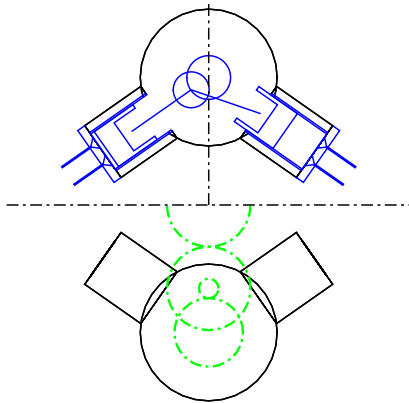


Figure 4 Piston engine arrangement inside core with piston assembly (top) and gear box (bottom).

Piston, cylinder liner, cylinder head, and casing sizes were based on empirical data from high performance motors [9]. The used correlations are illustrated in Figure 5 and based on piston bore d . The cylinder liner thickness was additionally varied linearly with piston power. The piston is divided into two parts, with the piston head having a solidity of 80 % and the

skirt on the bottom having a solidity of 30 %. Piston bore and stroke are equal (square engine). A lower stroke could reduce piston engine size and weight, but infers higher acceleration forces on piston, cylinder liner, crankshaft and mounts.

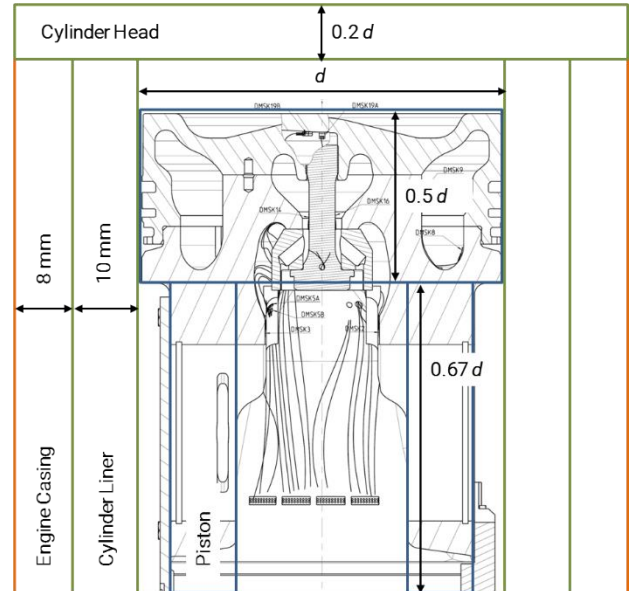


Figure 5 Piston, cylinder liner, cylinder head, and casing dimensions based on piston bore. The background shows a cutaway drawing from a high-performance piston [9].

The connecting rod between piston and crankshaft is 1.7 times as long as the stroke [10]. The connecting rod cross-sectional area is sized to receive the peak tension during combustion with a safety factor of 3. The crankshaft has a baseline diameter of 190 mm [9] and is scaled with torque $\tau^{1/3}$. Two inlet and outlet valves are used each. Although this infers higher valve and camshaft weight, a better scavenging efficiency can be achieved. The valves are actuated with camshafts, with an assumed shaft diameter of 50 mm.

The piston engine was assumed to be equipped with liquid cooling. Potential cooling fluids are lubricant oil or fuel. Water is limited around 370 K (depending on pressure and additives), which is too low for the conceived operating temperature of the coolant. The heat sink of the liquid cooling is modelled to be a fraction of the bypass mass flow, which is diverted through a liquid/air heat exchanger, rejecting the heat the bypass air, which is subsequently mixed again with the bypass flow.

To reduce interaction effects between turbo components and the piston engine, buffering volumes are introduced. One is located between HPC outlet and the piston engine inlet, and the second between piston engine outlet and Joule burner inlet. The volumes settle the fluctuations in pressure and mass flow rate resulting from instationary piston engine operation mode.

Piston engine performance was simulated with crankshaft angle resolved OD control volume method. Scavenging losses are included in the simulation. Mechanical losses of 4.5 % in the piston engine and 2 % for the gearing between HPC and PE were estimated. Pressure losses of 1 % in intake and exhaust duct each were assumed.

Intercooler

The intercooler model was adapted from [11]. Heat transfer calculations, external pressure losses calculations as well as the weight estimation were implemented without alteration. The geometric model was simplified to better fit the in-house simulation environment and only the involute spiral configuration was implemented for better engine integration.

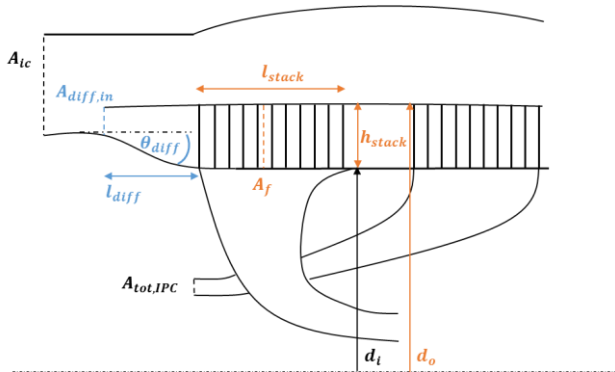


Figure 6 Intercooler geometry.

Parameters in black in Figure 6 are inputs from other components. The inner diameter (d_i) as well as the hot side inlet area ($A_{tot,IPC}$) are adapted from the IPC and the cold side inlet area (A_{ic}) from the fan. The blue parameters diffuser inlet area ($A_{diff,in}$), equivalent diffuser angle (θ_{diff}) and diffuser length (l_{diff}) are free design parameters and used to optimize the intercooler. The orange parameters are calculated. In addition to the shown geometric parameters, also performance characteristics such as the cold side

pressure loss and the heat exchanger effectiveness were calculated.

The internal pressure losses on the hot side were not calculated but set to the constant of $\pi_{ic,h} = 0.94$ as specified in [12]. Figure 7 shows the integration of the intercooler component into the overall engine model.

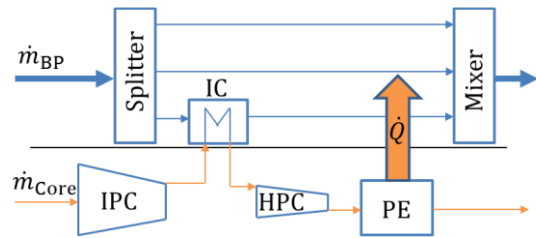


Figure 7 CCE IC schematic diagram of bypass flows.

On the hot side, the intercooler is placed between IPC and HPC. The cold side mass flow is modelled to be split into three streams: Stream one is the normal bypass mass flow. Stream two is used as cooling air for the piston engine. Stream three is fed to the intercooler cold side. All three streams are mixed before entering the bypass nozzle.

Flow path visualization

The flow path was visualized in a component-based bottom-up manner. The turbo components are plotted stage-wise with typical hub-to-tip ratios, gap ratios, aspect ratios, taper ratios and axial flow Mach numbers. The values were derived from a reference GTF general arrangement drawing and contemporary geared turbofan engines [13]. Relative duct lengths were correlated with relative radius reduction based on mean inlet radius. Radial compressor size was estimated with correlations from [14].

The piston engine crankshaft casing inner radius is assumed to be 1.5 times the piston engine stroke. The buffering volume was conceived as a torus. It was ensured that the buffering volume before the piston engine fits into the core cowling boundary, and the volume after the piston engine fits into the space between the two piston engines. Nozzles are assumed to have an inclination of 12° for the inner core cowling and 20° for the core nozzle.

All components are then arranged in sequential order by propagating their boundary point coordinates to the adjacent components. If

multiple conditions are present for a component, the critical condition is identified and applied. For example, the combustor is placed within the piston engines inner circle, if possible, and otherwise behind the piston engine.

Weight estimation

Engine weight for the year 2050 reference GTF was estimated within the ULTIMATE project. To remain consistent with the modelling of the reference engine weight, scaling of component weights based on first order principles is pursued.

Compressors, turbines, nozzles, combustors were scaled with logarithmic mean corrected mass flow and stage count n_{st} :

$$m_{CCE} = m_{GTF} \cdot \frac{\dot{m}_{corr,mean,CCE}}{\dot{m}_{corr,mean,GTF}} \cdot \frac{n_{st,CCE}}{n_{st,GTF}} \quad (1)$$

with corrected mass flow rate

$$\dot{m}_{corr} = \dot{m} \cdot \frac{\sqrt{\frac{T}{T_{std}} \cdot \frac{R}{R_{std}}}}{\frac{p}{p_{std}}} \quad (2)$$

with $T_{std} = 288.15$ K, $p_{std} = 101.325$ kPa and $R_{std} = 287.05 \frac{J}{kg \cdot K}$, and averaging of mass flow with the component entry condition 1 and exit condition 2:

$$\dot{m}_{mean} = \frac{\dot{m}_{corr,1} - \dot{m}_{corr,2}}{\ln(\dot{m}_{corr,1}) - \ln(\dot{m}_{corr,2})} \quad (3)$$

Shafts were scaled with torque τ , assuming geometrically similar scaling of the shaft

$$m_{CCE} = m_{GTF} \cdot \left(\frac{\tau_{CCE}}{\tau_{GTF}} \right)^{\frac{2}{3}} \quad (4)$$

The gearbox was sized based on power P and gear ratio q_n with exponents according to [15]

$$m_{CCE} = m_{GTF} \cdot \left(\frac{P_{CCE}}{P_{GTF}} \right)^{0.75} \cdot \left(\frac{q_{n,CCE}}{q_{n,GTF}} \right)^{0.15} \quad (5)$$

Bearings and accessories were scaled linearly with thrust

$$m_{CCE} = m_{GTF} \cdot \frac{F_{CCE}}{F_{GTF}} \quad (6)$$

Since fan diameter was kept constant, fan and nacelle weight were assumed to be constant, too. This assumption may be a minor simplification, since the fan in the CCE has a lower specific thrust and, hence, might be slightly lighter.

All components not present in the GTF are modelled in a bottom-up manner. This concerns the piston engine, the intercooler and the piston engine gearbox. Piston engine weight is estimated by calculating component weight with the volume obtained from the conceptual design described in section 3-2 and the material densities. The material envisaged for each of the parts is summarized in Table 2. Most parts are assumed to be manufactured from steel-based alloys. The piston is envisaged with TiAl for lower weight, and the cylinder block with the magnesium alloy AZ31. The obtained weights with the presented methodology have been validated against published total engine weight data with a mean error of 10% [8].

Intercooler weight is estimated as a function of its volume, the required wall thicknesses with titanium as material.

Table 2 Piston engine materials and their properties.

Component	Material	Density [kg/m ³]
Liner, connecting rod, cylinder head, crankshaft, camshaft, upright shaft	Steel	7 730
Cylinder Block	AZ31	1 800
Piston	TiAl	4 000

NOx emissions

For the piston engine, a time-resolved reaction kinetic 2-zone model was developed and validated [16]. The logic of the 2-zone model is illustrated in Figure 8. Zone 1 is the unburned zone with fresh air. Zone 2 contains the combusted air. Until start of combustion, all air in the cylinder is in Zone 1. Once ignition starts, zone 2 is initiated through mass flow from the flame front (which is assumed to be infinitely small), and later progressively through mixing with Zone 1. At the end of combustion, both zones are assumed to be perfectly mixed.

The reactions considered for NO_x creation are the extended Zeldovich mechanism [16] shown in Equations (7) to (9).



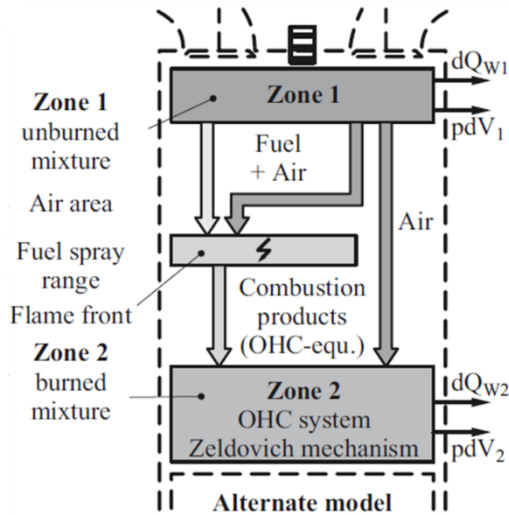


Figure 8 2-Zone model operating logic [16].

The reactions were integrated based on the time-resolved process parameters obtained from a 0D piston model. Reaction kinetic constants were taken from GRI-MECH 3.0 [17] and the fluid properties from the NASA Chemical Equilibrium with Applications database [18, 19]. For validation, 5 engines have been used, which had both performance and NO_x emission simulation results available [20, 21, 22, 23, 24]. The results of one four stroke engine are illustrated in Figure 9. As can be seen, the absolute values and trends can be well replicated with the NO_x emissions simulation. Some uncertainty is incurred in the performance modelling of the engines, since usually not all relevant parameters are published. The uncertainty found during calibration is used in the results in Section 4.3 to provide an averaged value for the expected NO_x emissions within the calculated range.

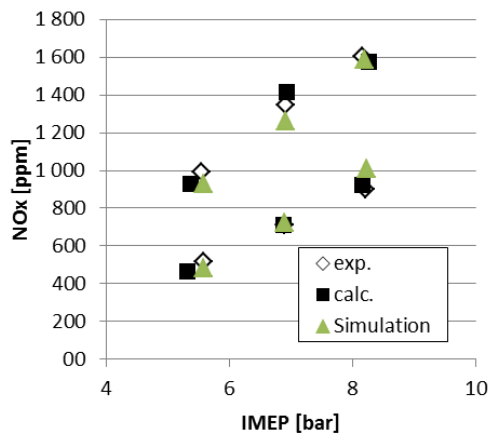


Figure 9 NO_x 2-zone model validation for a four stroke diesel engine [22].

For conventional combustor NO_x emission an established semi-empirical correlation was used [25]. It depends on the combustion chamber inlet conditions T_{35} and p_{35} for the NO_x severity parameter s_{NOx} :

$$s_{NOx} = \left(\frac{p_{35}}{2964.5 \text{ kPa}} \right)^{0.4} \cdot e^{\left(\frac{T_{35}^* - 826.26 \text{ K}}{194.39 \text{ K}} \right)} \quad (10)$$

To obtain the emissions index (EINO_x), a calibration factor for modern lean direct injection combustors as found in [1] was used:

$$EINOx = 12.4 \cdot s_{NOx} \quad (11)$$

Since the conventional combustor is operated on vitiated air, the combustor inlet temperature T_{35} is corrected to the equivalent inlet temperature for fresh air T_{35}^* . The logic of the assessment is illustrated in Figure 10. This approach ensures that the same flame temperature is achieved as in the case of fresh air, where NO_x is mainly produced.

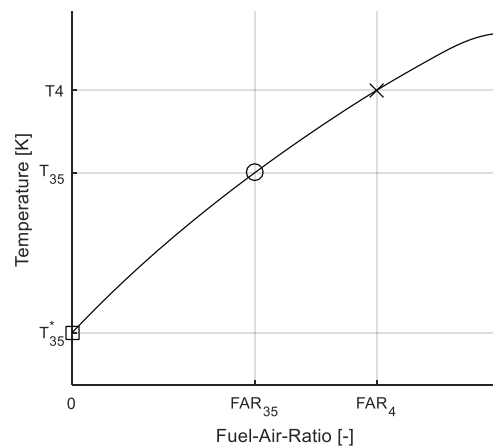


Figure 10 Temperature over fuel-air-ratio diagram for equivalent combustor inlet temperature estimation.

4 Results

4.1 Engine Performance

Design study

Both CCE versions were optimized towards minimum fuel burn. All design parameters are listed in Table 3. For the non-intercooled version only T_4 and OPR are relevant.

Table 3 CCE design study parameters

Intercooler		Engine	
Fixed parameters	Value	Study parameters	Value
$M_{tubes,h}$ [-]	0.07	T_4 [K]	1400 – 1800
n_{stacks} [-]	24		
$l_{Diffusor}$ [m]	0.4	OPR [-]	40 – 70
Optimization parameters	Limits		
$\theta_{Diffusor}$ [rad]	0.05 – 0.2	ϵ_{IC} [-]	0.4 – 0.7
f_{pi} [-]	1 – Inf		

The resulting parameters of the baseline CCE and its performance in the three most relevant operating points ToC, TO and CR are shown in Table 4. The engine design was constrained by the peak pressure of 300 bar in TO, and the piston exhaust temperature T_{34} in both TO and ToC. The maximum permissible piston bore was set to 0.20 m to ensure placement within the core cowl.

Table 4 CCE operating conditions

Parameter	ToC	TO	CR
Thrust [kN]	49.73	182.84	32.87
T_4 [K]	1700	1764	1432
OPR [-]	38.0	28.9	31.3
BPR [-]	33.7	35.8	36.5
TSFC [g/kN/s]	12.38	6.89	11.51
T_3 [K]	719	725	630
T_{34} [K]	1395	1392	1019
Π_{PE} [-]	1.80	1.65	1.46
p_{peak} [bar]	189	300	174
Π_{IPC} [-]	3.4	3.0	3.1
Π_{HPC} [-]	5.6	5.4	6.2

Unless declared otherwise, the study parameters and boundary conditions for the intercooled CCE are identical to those of the non-intercooled CCE (s. above). As starting point the final thrust values from the baseline CCE were used (Table 4). The intercooler is optimized towards minimum cold side pressure loss while still providing the required effectiveness.

Figure 11 is an exemplary exhibit of the T_4 -OPR optimization performed on each IC and their respective effectiveness (ϵ_{IC}). Different IC effectiveness result in varying optimal OPRs but the largest T_4 was always most beneficial with regards to the overall fuel burn.

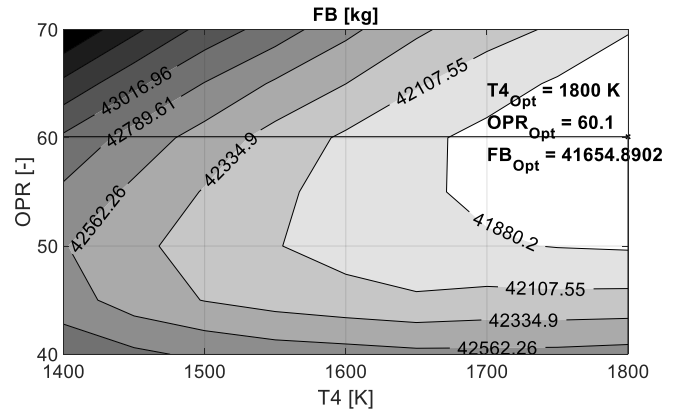


Figure 11 Mission fuel burn optimization for $\epsilon_{IC} = 0.6$.

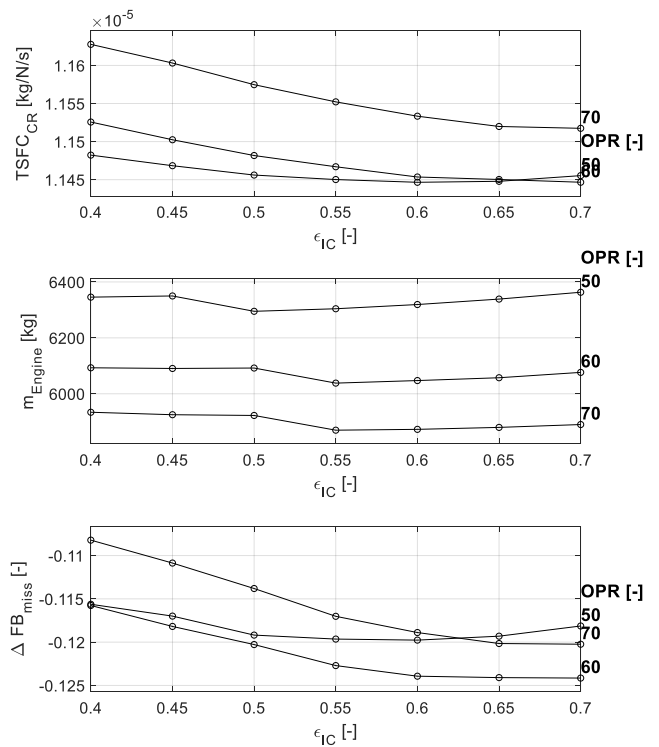


Figure 12 CCE IC performance optimization $T_4 = 1800K$.

Figure 12 shows the results of the overall engine fuel burn optimization with regards to ϵ_{IC} and OPR at the highest possible T_4 of 1800 K. It was limited to not exceed a maximum T_4 of 1920 K during TO. Increasing OPR leads to lower engine weights. However, the fuel burn benefit from an engine with an OPR of 70 is outweighed by its increased TSFC. The optimal engine configuration uses an intercooler with an effectiveness of 0.6, a T_4 of 1800 K and an OPR of 60.

Based on the previously selected configuration the thrust requirements due to the weight decrease compared to the baseline CCE

were adjusted and lead to the optimal operating conditions shown in Table 5.

Table 5 CCE IC operating conditions.

Parameter	ToC	TO	CR
Thrust [kN]	48.59	178.95	32.02
T_4 [K]	1800	1905	1533
OPR [-]	60.0	45.2	49.1
BPR [-]	37.7	40.7	40.7
TSFC [g/kN/s]	12.16	6.88	11.45
T_{34} [K]	1310	1291	1016
Π_{PE} [-]	1.80	1.62	1.52
p_{peak} [bar]	189.0	300.0	150.6
Π_{IPC} [-]	5.94	5.57	5.41
Π_{HPC} [-]	5.52	4.86	5.88
ϵ_{IC}	0.60	0.67	0.62
$\Pi_{IC,c}$ [-]	0.95	0.96	0.95

Off-design performance

In this section, the part load behavior of the CCE is illustrated. The CCE adds versatility to part load operability, because the piston engine provides a new degree of freedom. For cruise, it is assumed that cooling air flow can be reduced by 50 % with active cooling air control, because the temperature levels are very low with T_4 around 1400 K, so only sealing air is required.

A very flat part power fuel consumption can be achieved as shown in Figure 13 (a). This is partially achieved through a shift in fuel split from the conventional combustor (CC) to the

piston engine. As shown in Figure 13 (b), the ratio of fuel injected in the piston engine increases progressively from 57 % to 67 % going into part load.

4.2 Conceptual Design

Weight

Engine weight is evaluated according to the methods described in section 3-2. The results for the CCE are listed in Table 6. Total engine weight increases by 1858 kg, or 35.5 %. The consolidated weight of all conventional turbo components decreases by 522 kg, mainly by reducing HPC size from 11 stages to 3+1 radial stage, and by reducing turbine weights in total by about half. The piston engine adds 2292 kg to the total engine weight, which constitutes about 32 % of the total engine weight.

The addition of an intercooler to the CCE results in an overall 1372 kg lighter engine compared to baseline CCE – a weight decrease by 19 %. The main weight benefits stem from the smaller piston engine. The intercooler adds 121.3 kg to the total engine weight. The increased OPR leads to a more compact core engine in general and results in weight benefits for all components in the core flow path. A comparison between GTF, CCE and CCE IC is visualized in Figure 14.

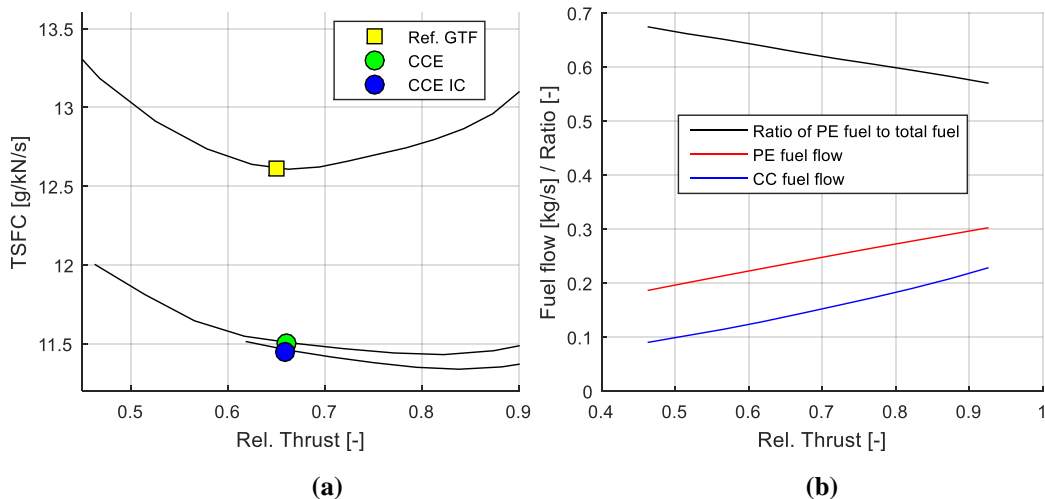


Figure 13 CCE part load behaviour at cruise conditions with (a) fuel consumptions and (b) fuel flow split between piston engine and combustor.

Table 6 Weight comparison between GTF, CCE and CCE IC

Weights [kg]	Ref. GTF	CCE	Δ [%]	CCE IC	Δ vs CCE [%]
Turbo engine	3613.4	3096.8	-14.3	2900.2	-6.3
Nacelle	1633.4	1633.4	0	1633.4	0
PE Gearbox	0	88	-	73.9	-16.0
Piston Engine	0	2291.8	-	1252.6	-45.3
Intercooler	0	0	-	121.3	-
Total	5246.8	7382.2	+40.7	6009.5	-18.6

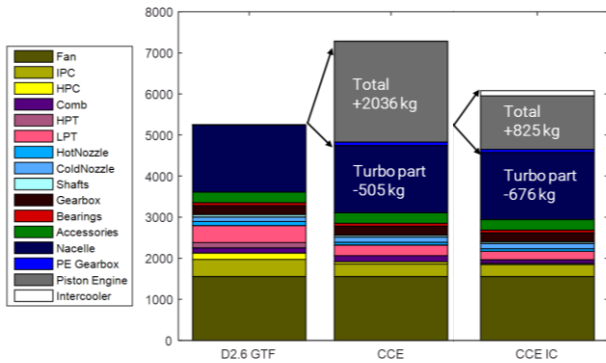


Figure 14 Weight comparison of GTF, CCE and CCE IC

The resulting engine general arrangement is shown in Figure 15. Total engine length increases by 0.54 m. Although the piston engine is 1.55 m long, a large fraction can be compensated through reduced HPC length. The outer piston engine crankshaft casing violates the core cowling perimeter. As can be seen in Figure 15 (right), the violation affects only a minor fraction of the circumference. A more compact arrangement may be able to omit this violation. Otherwise, an excrescence with aerodynamic

fairing is required at this point, which might result in added bypass duct losses.

Turbo component size is visibly reduced due to the reduced core mass flow rate ($-46\% \dot{m}_{25}$). The dashed circles indicate the buffering volumes. The piston engine exhaust buffering volume is enclosed by the two banks of the piston engine. The combustor is slightly inward angled to allow for a more compact arrangement with the piston engine.

Figure 16 shows the general arrangement drawing of the CCE with intercooler versus the baseline. The implementation of the intercooler with a total length of 1.03 m only results in a 0.23 m increase in engine length. This is partly because the intercooler is placed outside the direct core flow path and the piston engine is considerably smaller. The visualization of the intercooler does not include inflow and outflow ducts on the hot side and neither the outflow duct on the cold side. Additional space has been reserved for these components. A more detailed drawing of the intercooler is presented in [11]. The intercooler might also require a slight modification of the bypass duct to minimize pressure losses.

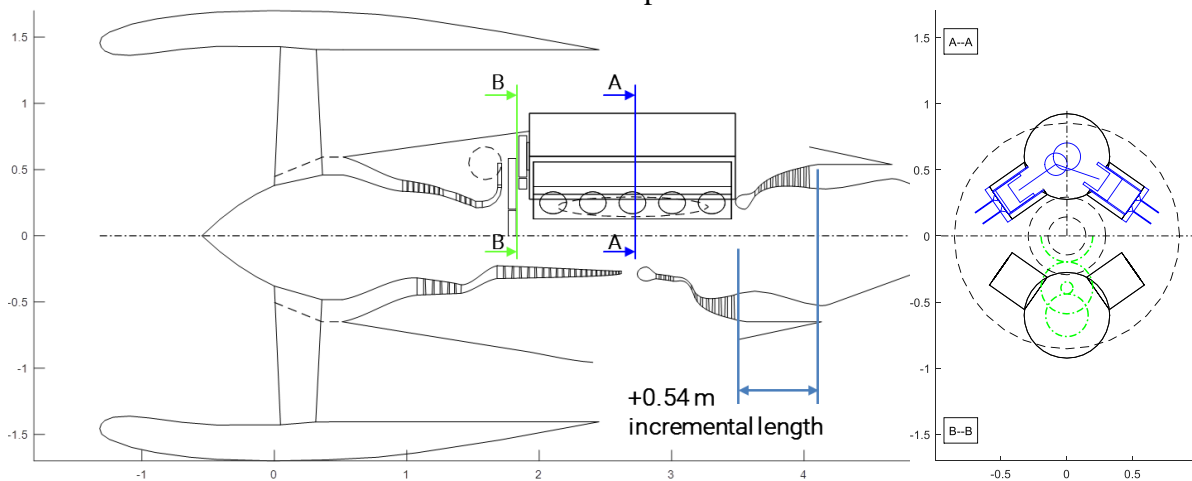


Figure 15 General arrangement drawing of the CCE (left, top) in contrast to the reference GTF (left, bottom). Sectional view of piston engine internals (right, top) and piston engine gear box (right, bottom)

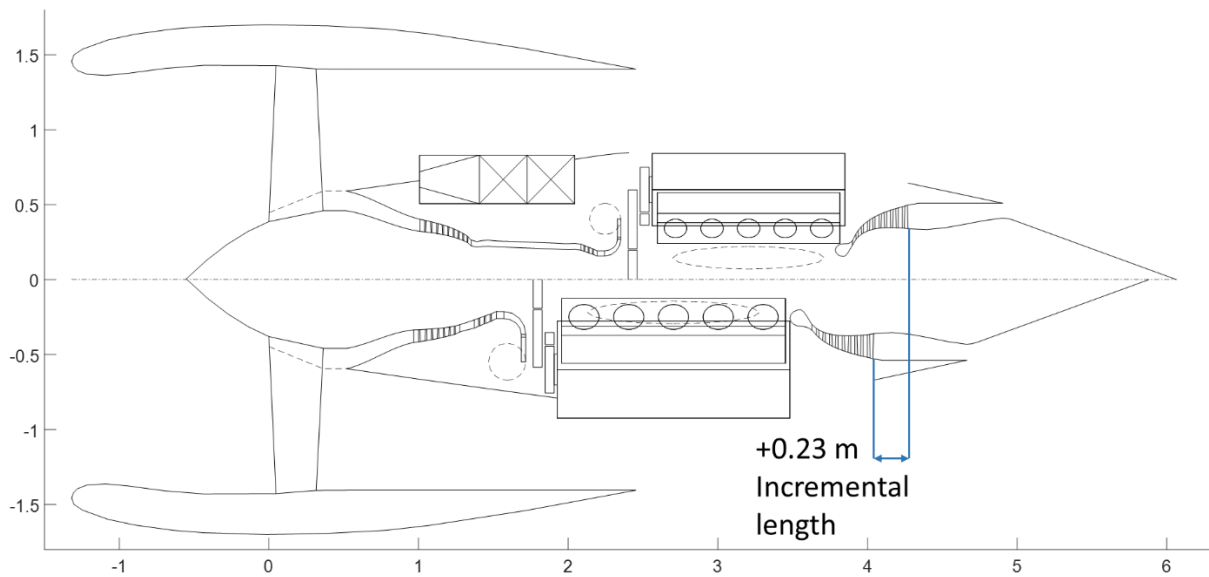


Figure 16 General arrangement drawing of the CCE with IC (top) in contrast to the CCE (bottom)

4.3 Concept Evaluation

Fuel burn

Mission fuel burn is estimated according to the methodology presented in [7]. It includes the effects of TSFC in the relevant mission points, fan diameter and engine weight. The values used for evaluation are summarized in Table 7. The CCE achieves a total improvement of 9.6 %. Revoking the piston engine size restriction (“CCE Large”) results in a considerably heavier engine but also a 2.3 % better fuel burn than the baseline CCE, despite the added engine weight. Therefore, a larger core engine is clearly desirable in terms of fuel burn, but needs to be evaluated in terms of size, cost and dynamic loads. The CCE IC has a higher improvement of

12.5 %, by virtue of lower engine weight. The results are visualized in Figure 17. As can be seen, the added engine weight consumes about 5 % fuel burn improvement. This constitutes the maximum improvement potential in piston engine weight savings.

The ULTIMATE target of -15 % is not achieved with the presented engines. However, considerable optimization potential still lies in the CCE architecture. The piston engine provides a wide parametric space that allows for further optimization, e.g. valve timings, heat release characteristics, and compression ratio. The intercooled CCE comes closest to the target and the benefit through piston engine weight reduction is notable.

Table 7 Fuel burn assessment summary

Parameter	Optimized GTF	CCE	CCE large	CCE IC
TSFC _{ToC} [g/kN/s]	13.73	12.38	12.09	12.16
TSFC _{CR} [g/kN/s]	12.62	11.51	11.23	11.45
TSFC _{TO} [g/kN/s]	8.28	6.89	6.70	6.88
d_{Fan} [m]	2.840	2.867	2.867	2.867
m_{PPS} [kg]	5161.3	7283.2	7665.5	6009.5
ΔFB vs Y2050 GTF [%]	-1.5	-9.6	-11.9	-12.5
ΔFB vs Y2000 [%]	-45.8	-50.3	-51.5	-51.9

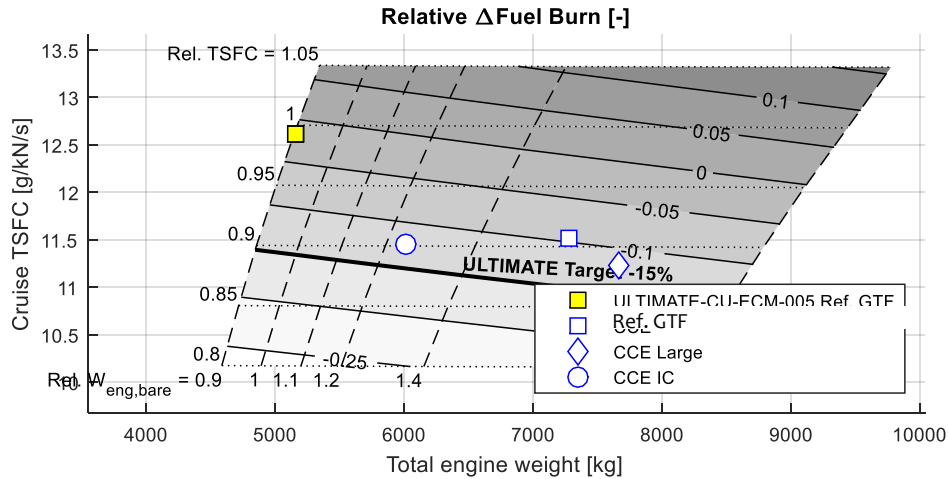


Figure 17 Fuel burn assessment visualisation for CCE and CCE IC.

NO_x emissions

The estimated emissions for the CCE and the intercooled CCE are shown in Table 8. The ranges shown for the piston engine are lower and upper bounds due to simulation uncertainty as described in Section 3-2. The ULTIMATE target of -20 % was partially achieved by the intercooled engine. Emissions were estimated to improve by 12 % on average compared to the reference GTF. The non-intercooled version has 15 % higher NO_x emissions than the GTF.

CAEP/6-75 % targets are missed in both cases. The CCE exceeds the emission target by 267 % and the intercooled CCE by 80% based on OPR. The intercooled CCE has a 66% greater certification limit than the baseline, because of increased OPR. Both engines comply with an emission target derived from the peak piston engine pressure. The CCE emits 55 % less NO_x than the p_{max} target and the intercooled CCE has

66 % less emissions. In the spirit of the NO_x emissions regulations, which allow for higher NO_x emissions by more fuel-efficient engines (expressed though increased OPR), an emissions regulation between both presented reference pressure ratios is warranted.

During cruise flight both CCE versions have higher NO_x emissions than the reference GTF. For the CCE, it is 181 % larger and for the intercooled CCE 97 %. Notably, the CCE performs comparably worse in part load than in full load. The emissions in part load are still relatively high, because peak pressures and temperatures in the piston engine do not reduce as much as they do in a turbofan. This finding suggests that part load operation of the piston engine requires further investigation with special focus on NO_x emissions, which may be reduced through optimized valve and injection timings.

Table 8 CCE NO_x emissions

FN	CCE				CCE IC			
	SLS 100%	SLS 85%	SLS 30%	Cruise	SLS 100%	SLS 85%	SLS 30%	Cruise
t [s]	42	132	240	-	42	132	240	-
EINO _{XCC} [g/kg]	1.26	0.98	0.20	0.21	1.05	0.51	0.26	0.09
EINO _{XPE} [g/kg]	76.40	76.96	63.22	69.52	72.18	66.87	76.50	54.89
Dp [g/s]	66.0	57.3	17.1	16.56	53.42	34.44	17.80	11.65
Dp_{tot} [g]	14447			-	11062			-
ΔDp_{tot} vs GTF [%]	14.6			+181*	-12.2			+97*
CAEP/6-75% OPR [g]	3980	Δ [%]	267.3	-	6125	Δ [%]	80.6	-
CAEP/6-75% p_{max} [g]	32754	Δ [%]	-55.4		32754	Δ [%]	-66.2	

* Cruise Δ for Dp instead of Dp_{tot}

5 Conclusion

The investigations for the Composite Cycle Engine (CCE) verified that the technology has a significant fuel burn improvement potential. The baseline engine improves fuel consumption by 9.6 %. The cruise TSFC improves by 8.8 %, while total engine weight increases by 41 %, or 2100 kg. Engine length increases moderately by 0.54 m. Although the piston engine occupies a larger space, the turbo component sizes (mainly HPC) reduce considerably. An option to leave piston engine size unrestricted revealed a further fuel burn improvement potential of 2.3 %, at the cost of 400 kg added engine weight. Using an intercooler in combination with the CCE concept shows multiple positive effects: An additional fuel burn improvement of 2.5 % furthermore increases the CCE's efficiency. The engine is considerably lighter by 1270 kg, and has therefore cost advantages over the baseline that are most likely going to outweigh the additional costs for the intercooler.

The NO_x emissions of the baseline CCE in the LTO cycle are on average 15 % higher than the GTF emissions. This may be permissible considering the reduced CO₂ emissions, but piston engines are not considered in the certification regulations. The intercooled CCE has 12 % lower estimated NO_x emissions on average than the GTF, and because of the greater OPR significantly increased permissible emissions. Therefore, the chance to meet NO_x certification targets is higher. In cruise, simulated NO_x emissions are 181 % higher than the GTF's for the CCE, and 97 % for the intercooled CCE. This warrants a higher attention to cruise operating conditions of the piston engines. An adaptation of valve and heat release timings might alleviate these results considerably. Otherwise, efficiency might need to be traded against NO_x emissions, if altitude emissions become part of the regulation.

Acknowledgements

The studies were conducted in the project ULTIMATE ("Ultra Low emission Technology Innovations for Mid-century Aircraft Turbine Engines"). This project received

funding from the European Union's Horizon 2020 research and innovation programme under grant agreement No 633436.

References

- [1] v. d. Bank, R. et al. Advances in ultra-high pressure ratio core-engines. 65. *Deutscher Luft- und Raumfahrtkongress*. DLRK2016-420006. September 2016.
- [2] Advisory Council for Aviation Research and Innovation in Europe (ACARE). *Realising Europe's Vision for Aviation*. Strategic Research and Innovation Agenda. Vol. 1. Brussels, Belgium, Sept. 2012, pp. 145–147
- [3] Grönstedt, T. et. al. Ultra Low Emission Technology Innovations for Mid-Century Aircraft Turbine Engines, ASME Turbo Expo 2016, GT2016-56123, Seoul, South Korea, June 2016.
- [4] S. Kaiser, S. Donnerhack, A. Lundbladh, A. Seitz, "Composite Cycle Engine Concept with Hectopressure Ratio", *Journal of Propulsion and Power*, Vol. 32, No. 6, 2016. doi: 10.2514/1.B35976
- [5] Sascha Kaiser, Arne Seitz, Patrick Vratny, and Mirko Hornung. Unified thermodynamic evaluation of radical aero engine cycles. In *Proceedings of the ASME Turbo Expo 2016*, number GT2016-56313, Seoul, South Korea, June 2016. doi:10.1115/GT2016-56313.
- [6] P. Eilts, J. Friedrichs, "Investigation of a Diesel Engine for Aircraft Application", AIAA Propulsion and Energy Forum, Atlanta, GA, USA, July 2017. doi: 10.2514/6.2017-4792
- [7] Philipp Heinemann, Periklis Panagiotou, Patrick Vratny, Sascha Kaiser, Mirko Hornung, and Kyros Yakinthos. Advanced tube and wing aircraft for year 2050 timeframe. In *55th AIAA Aerospace Sciences Meeting*, number AIAA 2017-1390, Grapevine, Texas, January 2017. doi:10.2514/6.2017-1390.
- [8] Paul Keller, "Piston engine conceptualization for composite cycle engines", Master's Thesis, TU Munich, May 2017
- [9] S. G. Schneider, „Mechanische und thermische Beanspruchung in Großdieselmotoren bei extrem hohen Mitteldrücken“, Dissertation, TU Munich, 2012.
- [10] Van Basshuysen, R., and Schäfer, F., "Handbuch Verbrennungsmotor", 5th ed.,

- Springer Fachmedien, Wiesbaden, Germany, 2015.
- [11] Zhao, X., Grönstedt, T., and Kyprianidis, K. G., "Assessment of the Performance Potential for a Two-Pass Cross Flow Intercooler for Aero Engine Applications," XXI International Symposium on Air Breathing Engines, ISABE Paper 2013-1215, Busan, ROK, Sept. 2013.
- [12] Sascha Kaiser, Markus Nickl, Christina Salpingidou, Zinon Vlahostergios, Stefan Donnerhack, and Hermann Klingels, „Investigations of synergistic combination of the composite cycle and intercooled recuperation”, 23rd International Symposium of Air Breathing Engines, ISABE-2017-21451, Manchester, UK, September 2017.
- [13] G. R. Kappler, S. Staudacher, „Gewichtsstudie zu Niederdrucksystemen moderner Turbofan-Triebwerke“, 61. Deutscher Luft- und Raumfahrtkongress, 2012.
- [14] H. Grieb, "Verdichter für Turbo-Flugtriebwerke", 1st Ed., Springer-Verlag, Berlin, 2009.
- [15] Eric S. Hendricks, Michael T. Tong, "Performance and weight estimates for an advanced open rotor core-engines", TM-2012-217710, NASA Glenn Research Center, Cleveland, OH, September 2012.
- [16] G. P. Merker, C. Schwarz, G. Stiesch, F. Otto, „Simulating Combustion“, Springer-Verlag, Berlin, 2006.
- [17] Robert J. Kee, Fran M. Rupley, Ellen Meeks, and James A. Miller. "Chemkin-iii - a fortran chemical kinetics package for the analysis of gas-phase chemical and plasma kinetics", Technical Report UC-405, Sandia National Laboratories, Livermore, CA, May 1996.
- [18] Gordon, S., and McBride, B. J., 1994, Computer Program for Calculation of Complex Chemical Equilibrium Compositions and Applications - Part I: Analysis, Cleveland, Ohio.
- [19] McBride, B. J., and Gordon, S., 1996, Computer Program for Calculation of Complex Chemical Equilibrium Compositions and Applications - Part II: User Manual and Program Description, Cleveland, Ohio.
- [20] J. Mohammadhassani, Sh. Khalilarya, M. Solimanpur, A. Dadvand, "Prediction of NO_x Emissions from a DI Diesel Engine Using Artificial Neural Network", Modelling and Simulation in Engineering, Volume 2012, 2012. doi:10.1155/2012/830365
- [21] V. T. Lamaris, D. T. Hountalas, T. C. Zannis, S. E. Glaros, "Development and Validation of a Multi-Zone combustion Model for Predicting Performance Characteristics and NO_x Emissions in Large Scale Two-Stroke Diesel Engines", ASME 2009 International Mechanical Engineering Congress & Exposition, IMECE2009-11382, Lake Buena Vista, Florida, USA, November 2009.
- [22] C. D. Rakopoulos, D. C. Rakopoulos, D. C. Kyritsis, "Development and Validation of a Comprehensive Two-Zone Model for Combustion and Emissions Formation in a DI Diesel Engine", International Journal of Energy Research, No. 27, pp. 1221-1249, 2003. doi: 10.1002/er.939
- [23] L. Goldsworthy, "Real time model for oxides of nitrogen emissions from a slow speed marine diesel", Journal of Marine Engineering & Technology, No. A2, pp. 3-12, 2003. doi: 10.1080/20464177.2003.11020166
- [24] A. Andreasen, S. Mayer, "Modelling of the Oxidation of Fuel Sulfur in Low Speed Two-Stroke Diesel Engines", CIMAC Congress 2010, Bergen, 2010.
- [25] Kurzke, J., "GasTurb 11 - Design and Off-Design Performance of Gas Turbines", Germany, 2007.

8 Contact Author Email Address

kaiser.sascha@gmail.com
hagen.kellermann@bauhaus-luftfahrt.net

Copyright Statement

The authors confirm that they, and/or their company or organization, hold copyright on all of the original material included in this paper. The authors also confirm that they have obtained permission, from the copyright holder of any third party material included in this paper, to publish it as part of their paper. The authors confirm that they give permission, or have obtained permission from the copyright holder of this paper, for the publication and distribution of this paper as part of the ICAS proceedings or as individual off-prints from the proceedings.